

**Self-assembled monolayer of alkanephosphoric acid on nanotextured Ti**Sylvain Clair,<sup>1,2</sup> Fabio Variola,<sup>1,3</sup> Mykola Kondratenko,<sup>2</sup> Pawel Jedrzejowski,<sup>4</sup> Antonio Nanci,<sup>3</sup> Federico Rosei,<sup>1,a),b)</sup> and Dmitrii F. Perepichka<sup>2,a),c)</sup><sup>1</sup>*INRS-EMT, Université du Québec, 1650 Boul. Lionel-Boulet, Varennes, Québec J3X 1S2, Canada*<sup>2</sup>*Department of Chemistry, McGill University, 801 Sherbrooke Street West, Montreal, Québec H3A 2K6, Canada*<sup>3</sup>*Laboratory for the Study of Calcified Tissues and Biomaterials, Faculté de Médecine Dentaire, Université de Montréal, Montreal, Québec H3C 3J7, Canada*<sup>4</sup>*Plasmionique Inc., 1650 Boul. Lionel Boulet, Varennes, Québec J3X 1S2, Canada*

(Received 29 November 2007; accepted 23 January 2008; published online 9 April 2008)

Surface modification of titanium and its alloys is of great importance for their practical application as biomedical implants. We have studied and compared assembly of dodecylphosphoric acid on commercial polished and on nanostructured titanium disks. The latter were produced by chemical etching that created nanoscale pits of typical size of about 20 nm. Enhanced hydrophobicity and high molecular density were obtained after functionalization of the nanotextured substrate. Aging tests showed a lifetime of the organic films of about one month in phosphate buffer. The samples were characterized by means of infrared spectroscopy, contact angle measurements, ellipsometry, and atomic force and scanning tunneling microscopies. © 2008 American Institute of Physics.  
[DOI: 10.1063/1.2876421]

**I. INTRODUCTION**

The performance of biomedical materials strongly depends on the first interactions occurring when the material's surface comes into contact with a biological environment.<sup>1,2</sup> Surface chemistry and topography are well known as two of the most important factors that influence biological reactions at the body-implant interface. It is therefore important to properly control and characterize the surface physicochemical features of biomaterials.<sup>3,4</sup> The recent development of nanomaterial science raised a large interest in understanding the influence of nanoscale properties of materials on the behavior of biomolecules.<sup>5,6</sup> In particular, it was shown that cellular adhesion can be governed by selective nanostructuring of biomaterials.<sup>7-9</sup> Self-assembly of molecular monolayers is another powerful approach to modify surface properties.<sup>10-12</sup> Thiol-based self-assembled monolayers (SAMs) on metals (mostly on gold) have been extensively studied and used as model systems for a variety of applications. In general, these highly ordered SAMs can alter surface electronic levels, hydrophobicity, and adhesive properties, and provide the surface with chemical functional groups.<sup>10-12</sup> For oxide surfaces, a variety of molecules including alkyltrichlorosilanes, phosphonates, and carboxylic acids can be grafted on the surface, although the resulting films are generally not as well ordered as alkanethiols on gold.<sup>13-17</sup> A recent interest has emerged for organic functionalization of the native oxide surfaces of tantalum, titanium, and related alloys in connection with their wide use as biocompatible materials, in particular, in implants.<sup>18,19</sup> For this purpose, phosphoric acid terminated alkyl chains were

shown as a good candidate for building SAMs on such materials because of their strong chemical bonding to surface oxides.<sup>20</sup> Most of previous studies<sup>21-24</sup> of alkylphosphonate films on titanium were performed on substrates consisting of Ti or TiO<sub>2</sub> thin films deposited on silicon wafers by physical vapor deposition (PVD). Contact angles as high as 110° were reported for these systems, demonstrating hydrophobic character close to what can be obtained for thiols on Au(111), the latter being considered as a perfectly well ordered system on an ideally flat surface.<sup>10-12</sup> However, similar functionalization of commercial Ti metal, which is more relevant to fabrication of bioimplants, leads to lower contact angles.<sup>25</sup>

Our goal is to combine a nanoscale modification approach with a chemical functionalization of the surface. This strategy is expected to deliver novel integration properties for biomaterials with improved performance.<sup>22,26</sup> In this article we investigate the effects of titanium nanoscale topography on the subsequent formation of dodecylphosphoric acid films. Nanoscale roughness was obtained on Ti disks by chemical etching in piranha solution, as reported previously.<sup>27</sup> This treatment yields a three-dimensional spongelike titanium oxide surface with an average pit size of 20 nm. We find that, on such surface, organic films with high molecular density and exhibiting enhanced hydrophobic behavior can form. Additionally, we show results on the effects of aging of the organic layer.

**II. MATERIALS AND METHODS**

The substrates consist of commercially pure grade 2 Ti disks (cpTi) with a diameter of 14 mm and a height of 2 mm, mechanically polished to a mirror finish to produce reproducibly flat substrates. Surface nanotexturing was obtained by a 2 h treatment in a 1:1 mixture of sulfuric acid (95%)–hydrogen peroxide (30%) (piranha solution), as described

a) Authors to whom correspondence should be addressed.

b) Electronic mail: rosei@emt.inrs.ca.

c) Electronic mail: dmitrii.perepichka@mcgill.ca.

elsewhere.<sup>27,28</sup> Great care should be exercised when preparing and handling this highly aggressive solution. The mixing is an exothermic process, and a violent decomposition reaction can occur when mixing large amounts of these chemicals.

Dodecylphosphoric acid was purchased from City Chemical LLC and dissolved in tetrahydrofuran (THF) (1 mM). Before deposition, the samples were briefly cleaned in concentrated sulfuric acid and rinsed with water and THF. Dodecylphosphoric acid (DDPA) films were prepared following a standard procedure.<sup>16,21–25,29,30</sup> The phosphoric acid solution was drop cast on the Ti disks. After solvent evaporation, the samples were heated in an oven at 130 °C for 24 h, a treatment that produces covalent binding of the molecules to the surface through Ti–O–P linkages.<sup>16,30</sup> The samples were then sonicated several times in THF to remove all physisorbed materials. The SAMs were characterized by means of static water contact angle measurement, ellipsometry (Gaertner L116C ellipsometer), infrared spectroscopy [Fourier transform infrared (FTIR), Thermo Nicolet 6700 spectrometer], and atomic force microscopy (AFM) in dynamic mode (Nanosurf Easyscan AFM) in ambient conditions. For the ellipsometric measurements, the reference substrate was taken as the equivalent molecule-free substrate (i.e., a substrate exposed to all pretreatment procedures except for covalent functionalization step). For ellipsometry and contact angle measurements, the indicated error margins were calculated from statistical measurements on five different locations on the disk and on three independently prepared samples. In ellipsometry measurements, a refractive index of 1.46 was assumed for the organic layer. In the case of nanotextured surfaces, we evaluated the influence of the nanoscale structure by modeling it with the Bruggeman effective medium approximation.<sup>31,32</sup> Calculations for the different models and parameter optimization were performed with NKDGEN software.<sup>33</sup> From the measured ellipsometric angles  $\Delta$  and  $\Psi$ , the layer thicknesses are usually extracted by considering a stacking of homogeneous flat layers. For rough systems, however, this layer model can be improved by adding a top roughness layer consisting of a mixed phase of material and voids. Here we used a roughness layer of 40 nm in thickness corresponding to the estimated depth of the oxide<sup>27</sup> as well as the largest pit size observed by scanning electron microscopy (SEM), and a void concentration of ~50% (a value commonly used<sup>32</sup> and which corresponds roughly to the pit concentration as observed by SEM in our samples). For the SAM deposited system, the roughness layer was changed to a ternary phase composed of oxide, SAM, and voids. This model thus provides a volume fraction estimation of the organic phase, and gives no information on the actual organization of the SAM film, whether it is a continuous monolayer or locally a multilayer. This volume fraction was converted to an equivalent thickness, which was then compared to the thickness obtained by considering a simple flat layer model. In both cases we found similar values. In the following, we chose to present systematically the data derived from a flat layer model, considering the higher uncertainty due to the large number of parameters in the roughness layer model.

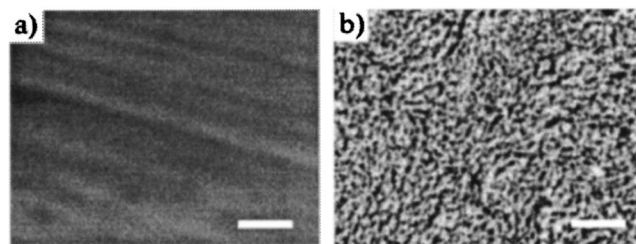


FIG. 1. SEM micrographs of the Ti surface; (a) smooth (polished); (b) after chemical etching (nanotextured). Scale bar 200 nm.

SEM analysis was carried using a JEOL-JSM-7400F field emission microscope operated at 1–2 kV. Scanning tunneling microscopy (STM) in ultrahigh vacuum (JEOL JSPM-4500) was performed on Ti foil samples (Alpha Aesar 99.5%, 0.25 mm thick) treated the same way as the disks. STM imaging of such oxide-covered titanium surfaces was typically done with a tunneling current of 30 pA and a sample bias voltage of 2 V.

### III. RESULTS AND DISCUSSION

#### A. Functionalization of smooth Ti surfaces

First we discuss the formation of DDPA SAMs on a smooth (polished, nonetched) substrate.

Commercial cpTi consists of polycrystalline grains with diameters of several microns. A native oxide layer, with a thickness of several nanometers, covers the Ti grains. This oxide layer is amorphous and irregular in thickness and chemical composition.<sup>27,34</sup> Figure 1(a) shows a high magnification SEM image of the substrate. The surface is smooth with no significant topographical features. Grooves resulting from the polishing process can be seen, but the regions between these grooves are essentially flat. After cleaning with concentrated sulfuric acid, water, and THF (to remove all physisorbed organic contaminants), control cpTi samples are only partially hydrophilic with water contact angle of  $46^\circ \pm 6^\circ$  (Table I) The “intrinsic” contact angle of the oxide surface on titanium is still controversial, and depends on the surface roughness (higher angle for flatter surfaces), oxide crystallinity, and contaminants.<sup>35</sup> Even after 2 min cleaning in oxygen plasma, which should burn off all organic impuri-

TABLE I. Summary of water static contact angle and ellipsometry data for dodecylphosphoric acid coated titanium. On nanotextured surfaces, the ellipsometry data correspond to an estimation of deposited organic material rather than a real film thickness (see details in Sec. II).

	Control	Coated
Contact angle smooth surface	$46^\circ \pm 6^\circ$	$88^\circ \pm 12^\circ$
Contact angle nanotextured surface	$0^\circ$	$120^\circ \pm 10^\circ$
Ellipsometry smooth surface	...	$20 \pm 10 \text{ \AA}$
Ellipsometry nanotextured surface	...	$80 \pm 30 \text{ \AA}$

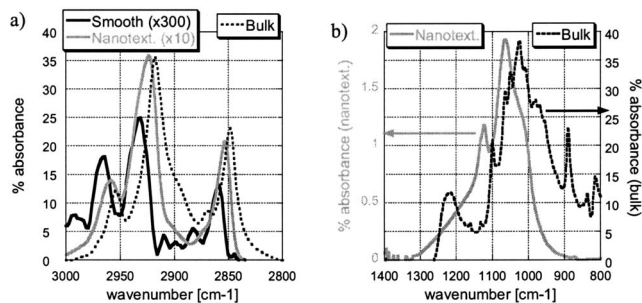


FIG. 2. IR spectra of DDPA films compared with the spectrum obtained from bulk material. (a) Aliphatic region (signal scaled by a factor 300 for films deposited on smooth substrate, and signal scaled by a factor 10 for films on nanotextured substrate). (b) PO region (left scale: nanotextured substrate, right scale: bulk); the signal was too low for films on smooth substrate and is not shown. See text for discussion.

ties (physisorbed and chemisorbed), but might also result in partial restructuring of the surface, the contact angle reduces only to  $32^\circ \pm 2^\circ$ .

After self-assembly of DDPA, the water contact angle increases to  $88^\circ \pm 12^\circ$  (Table I), demonstrating successful deposition of a hydrophobic molecular film. Previous studies on SAMs on titanium were mostly performed on Ti or  $\text{TiO}_2$  thin films deposited on silicon wafers by PVD, and water contact angles of  $110^\circ$ – $115^\circ$  were measured for dodecylphosphonates or longer alkyl chain SAMs.<sup>21–24</sup> The different nature of titanium oxide surfaces produced by PVD can explain the higher contact angles obtained. On commercial Ti disks, however, Quinones *et al.*<sup>25</sup> reported a value of  $96^\circ \pm 5^\circ$ , similar to what we have found.

The average SAM thickness of  $20 \pm 10 \text{ \AA}$  as measured by ellipsometry suggests that a monolayer of material was deposited (the theoretical length of straight molecules is  $18 \text{ \AA}$ ). The large error bar is due to inhomogeneities in the sample, as well as to sample-to-sample variations. The presence of hydrocarbon chains was confirmed by infrared spectroscopy, with characteristic peaks recorded at  $2933 \text{ cm}^{-1}$  ( $\text{CH}_2 \nu_{\text{asym}}$ ) and  $2858 \text{ cm}^{-1}$  ( $\text{CH}_2 \nu_{\text{sym}}$ ) [Fig. 2(a)].

Figures 3(a) and 3(b) show AFM images obtained, respectively, before and after phosphoric acid functionalization. In both cases, the root mean square (rms) roughness remains at 4 nm, and the overall aspect is qualitatively similar.

STM data after deposition are presented in Fig. 4. At low magnification [Fig. 4(a)], the presence of the organic film is not detectable, and the images exhibit no particular features. However, at high magnification [Fig. 4(b)], a cauliflowerlike structure is found, consisting of islands with a typical diameter of  $\sim 4 \text{ nm}$ . STM resolution on molecular systems can be remarkably enhanced when a single molecule is picked up by the tip.<sup>36</sup> We obtained high resolution images after applying a few voltage pulses of  $\sim 5 \text{ V}$  for 0.5 s. The molecular tip apex formed in this way was stable for several scans and could be easily formed again. In Fig. 4(b) individual molecules can be resolved. The corresponding corrugation (typically 0.05 nm high) presents a 0.7 nm pitch. This is larger than the intermolecular distance of 0.5 nm encountered in thiol-based

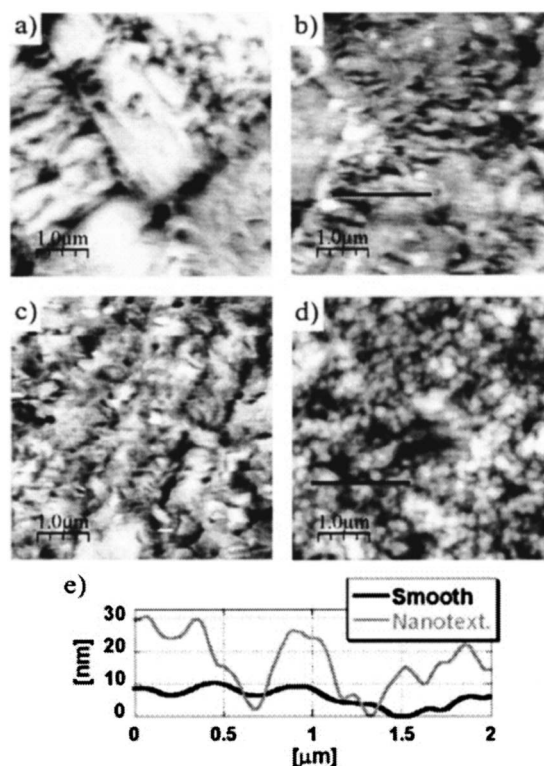


FIG. 3. AFM topographic images ( $5 \times 5 \mu\text{m}^2$ ) of Ti substrates; (a) smooth surface, clean; (b) smooth surface, coated with DDPA; (c) nanotextured surface, clean; (d) nanotextured surface, coated with DDPA; (e) height profiles along the lines in (b) and (d).

SAMs on Au(111).<sup>12</sup> However, similar spacing has been previously observed for SAMs on curved surfaces, for which an ordered structure was assumed.<sup>37,38</sup>

## B. Functionalization of nanotextured Ti surfaces

Here we discuss the formation of dodecylphosphoric acid films on the nanotextured (etched) substrate.

Figure 1 shows the effect of chemical etching on the texture of a titanium surface as observed by SEM. Whereas the untreated sample is smooth with no significant topographical features [Fig. 1(a)], a distinctive texture characterized by nanosized pits of about 20 nm is clearly seen on the etched surface [Fig. 1(b)].<sup>27</sup> The nanopits are uniformly distributed across the whole surface, and create a three-dimensional spongelike porosity.

Surface nanotexturing strongly affects its wetting properties. For the clean etched sample, the contact angle drops to  $0^\circ$  (see Table I). As compared to the nonetched one, the high hydrophilicity of this surface may be related to its porosity and/or to a composition change (e.g., hydroxylation<sup>39</sup>). However, because of its nanoroughness, this surface becomes highly hydrophobic when covered with an alkanephosphoric acid layer. Here a contact angle as high as  $120^\circ \pm 10^\circ$  is obtained (Table I), which is higher than what can be achieved on alkane-functionalized ideally flat surface (superhydrophobic effect<sup>40,41</sup>).

As mentioned in Sec. II ellipsometry on rough surfaces can only provide the volume fraction of organic material

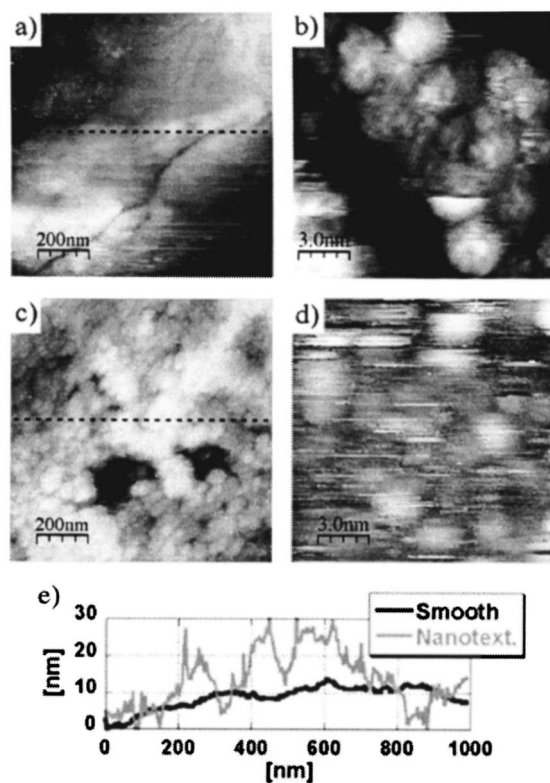


FIG. 4. STM topographic images (tunneling current 30 pA, sample bias 2 V) of DDPA covered titanium; [(a) and (b)] smooth substrate; [(c) and (d)] nanotextured substrate; (e) height profiles along the dashed lines in (a) and (c). In (b) molecular resolution is demonstrated with a 0.7 nm pitch.

deposited inside the nanopores, and cannot discriminate between mono- or multilayer formation. The data reveal an increase of quantity of deposited material (Table I). An equivalent thickness of  $80 \pm 30 \text{ \AA}$  was measured, considerably larger than the SAM thickness obtained on the smooth substrate. These data cannot objectively distinguish between the case where a monolayer is homogeneously formed on the high surface area of the nanotextured substrate and the case where multilayer islands are locally condensed. However, due to the difference between the molecular height (2 nm) and the substrate average pit size (20 nm), the binding behavior of DDPA molecules is expected to be similar on smooth and nanotextured surfaces. Considering the fact that previous studies showed that alkanephosphoric acid forms only monolayers on titanium,<sup>21–25</sup> we assume similarly the formation of a monolayer on this surface.

Infrared spectroscopy provides peaks for the  $\text{CH}_2$  groups recorded at  $2924 \text{ cm}^{-1}$  ( $\nu_{\text{asymm}}$ ) and  $2854 \text{ cm}^{-1}$  ( $\nu_{\text{symm}}$ ) [Fig. 2(a) and Table II]. In aliphatic molecules a blueshift of the  $\text{CH}_2$  stretching frequencies as a function of molecular environment has often been observed. This feature can be ascribed to various phenomena such as intramolecular conformational disorder,<sup>42,43</sup> surface coverage,<sup>44,45</sup> or a specific chemical environment.<sup>46</sup> Here the stretching frequencies increase gradually, from 2918 and  $2850 \text{ cm}^{-1}$  for the bulk solid material (DDPA), to 2924 and  $2854 \text{ cm}^{-1}$  for films on nanotextured substrate and to 2933 and  $2858 \text{ cm}^{-1}$  for SAM on a smooth substrate. Previous IR studies<sup>47</sup> have shown that

TABLE II. Comparison of IR peak positions corresponding to the methyl and phosphate group stretching modes for films grown on different substrates (DDPA=dodecylphosphoric acid, ODPA=octadecylphosphonic acid).

	$\text{CH}_2$ stretching ( $\text{cm}^{-1}$ )		PO stretching ( $\text{cm}^{-1}$ )
	$\nu_{\text{asymm}}$	$\nu_{\text{symm}}$	
DDPA/smooth Ti	2933	2858	<sup>a</sup>
DDPA/nanotextured Ti	2924	2854	1064
DDPA bulk	2918	2850	1025
DDPA solution in $\text{CCl}_4$	2926	2855	1030
ODPA/Ti (Ref. 25)	2914	2847	1012
ODPA/ $\text{TiO}_2$ (Ref. 45)	2917	2848	1075
ODPA/ $\text{TiO}_2$ (Ref. 14)	2918	2850	Not reported

<sup>a</sup>The signal is too weak.

the position of the  $\nu_{\text{asymm}}$  ( $\text{CH}_2$ ) peak is sensitive to the packing density of alkyl chains and indicates interchain interactions between long chains. Indeed, the solution of dodecylphosphoric acid in carbon tetrachloride reveals a vibration band at  $2926 \text{ cm}^{-1}$ , redshifted by  $8 \text{ cm}^{-1}$  from the solid material (Table II). Thus, differences in frequencies for aliphatic hydrocarbon groups reflect physical states of the phosphate monolayer on the surface, from a relatively densely packed phase on nanostructured Ti to a low density disordered film on flat polished Ti. The three-dimensional spongelike porosity of the nanotextured surface allows assembling of a large number of molecules, which create a dense molecular film with a high degree of interchain interactions between the alkyl chains. The relative increase of IR peak intensity [Fig. 2(a)] demonstrates that the quantity of organic material deposited on the nanostructured surface is significantly larger than on the smooth surface, thus confirming the ellipsometric findings. IR spectra in the phosphonate region [Fig. 2(b)] show blueshift of the P–O vibration frequencies in monolayers as compared to bulk material, thus indicating that phosphonate groups are covalently bound to titanium.<sup>25</sup> Table II summarizes the IR data and compares it with other studies found in the literature.

AFM imaging [Figs. 3(c) and 3(d)] reveals a threefold increase of rms roughness to 13 nm after chemical etching. The surface roughening is also visible by STM [Figs. 4(c) and 4(e)] where a very different structure is found at low magnification (increased roughness) as compared to the smooth surface. At higher magnification, however [Fig. 4(d)], a cauliflowerlike structure is also observed, suggesting a similar local organization of the molecules on the smooth and on the nanotextured surfaces.

### C. Aging effects

The stability of organic films is critical for their application in biomaterials, and should be carefully addressed. We have examined the degradation of the dodecylphosphonate films by measuring the water contact angle change over time. The samples were kept in ambient air or immersed in PBS 1X solution (phosphate buffered saline, an isotonic buffer solution commonly used in biochemistry) for several weeks and the results are summarized in Fig. 5. Some deterioration

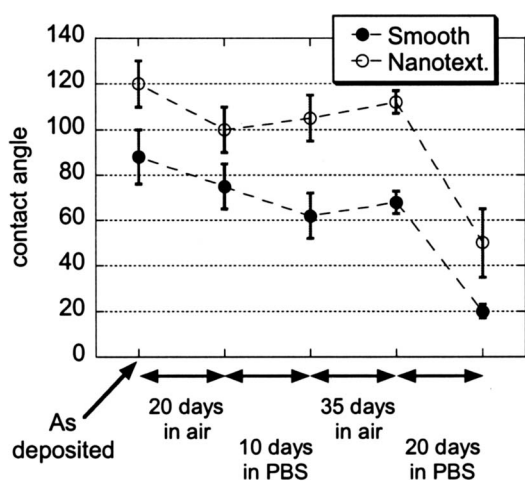


FIG. 5. Aging of DDPA films on titanium after keeping in air or in PBS solution. Filled circles: on smooth substrate; open circles: on nanotextured substrate.

of the hydrophobic properties of the films was observed after 20 days in air and 10 days in buffer solution, with contact angle decrease down to  $\sim 70^\circ - 75^\circ$  for the smooth substrate and to  $100^\circ$  on the etched one. No further degradation was encountered after an additional storage for one month in ambient air. However, prolonged (three more weeks) exposure of the samples to the buffer solution resulted in substantial decrease of the contact angle, revealing significant desorption of the organic film.

For thiol-based SAMs, spontaneous desorption can be observed within a few days of immersion in various solvents.<sup>48</sup> Film degradation results from oxidation or desorption from defect sites,<sup>49</sup> and can also depend on the solvent from which the film is formed.<sup>50</sup> In comparison, our alkanephosphoric acid films are relatively resistant to aging in a physiological-like environment. A further increase of their durability should be possible by optimizing film properties (e.g., by using longer alkyl chain molecules which should produce better molecular packing in the films<sup>43,51</sup>).

#### IV. CONCLUSION

In this article we investigated the effect of nanoscale texturing of titanium substrates on the subsequent formation of dodecylphosphoric acid films. The molecular self-assembly on smooth commercial cpTi disks is retarded as compared to the previously studied vacuum-deposited titanium films, as revealed by lower contact angle ( $88^\circ$ ). Nanotexturing of the cpTi disks was done by chemical etching with piranha solution that creates three-dimensional sponge-like nanoscale roughness. On such substrate, large amounts of molecules can be accommodated, thus forming organic film with high molecular density and presenting very high hydrophobicity (water contact angle  $\sim 120^\circ$ ).

Our latest results show that it is possible to finely control the thickness of oxide layer in Ti disks and the size of nanopits by varying the precise conditions of the chemical treatment.<sup>52</sup> We believe that the properties of organic films formed on such surfaces could be likewise adequately tuned. Recently, we made SAMs on Ti disks with a crystalline ox-

ide layer, which was created by annealing. In this case the formation of organic film was retarded and lower water contact angles were measured, suggesting significant influence of the substrate order on molecular self-assembly.

#### ACKNOWLEDGMENTS

We are grateful to Dr. C. Harnagea for help with AFM/STM imaging, to Dr. F. Vetrone for helpful discussions, and to S. F. Zalzal for help with SEM imaging. F.V. acknowledges graduate fellowships from CBIE (Canadian Bureau for International Education) and from FQRNT (Fonds québécois de la recherche sur la nature et les technologies). F.R. acknowledges partial salary support from FQRNT and from the Canada Research Chairs program. D.F.P. is grateful to DuPont USA for DuPont Young Professors Award. This work was supported by Plasmionique, Inc. and NSERC (Natural Sciences and Engineering Research Council of Canada) through a Collaborative Research and Development project.

- <sup>1</sup>D. A. Puleo and A. Nanci, *Biomaterials* **20**, 2311 (1999).
- <sup>2</sup>H. A. Liu and T. J. Webster, *Biomaterials* **28**, 354 (2007).
- <sup>3</sup>D. M. Ferris, G. D. Moodie, P. M. Dimond, C. W. D. Giorani, M. G. Ehrlich, and R. F. Valentini, *Biomaterials* **20**, 2323 (1999).
- <sup>4</sup>J. Auernheimer, D. Zukowski, C. Dahmen, M. Kantlehner, A. Enderle, S. L. Goodman, and H. Kessler, *ChemBioChem* **6**, 2034 (2005).
- <sup>5</sup>F. Rosei, M. Schunack, Y. Naitoh, P. Jiang, A. Gourdon, E. Laegsgaard, I. Stensgaard, C. Joachim, and F. Besenbacher, *Prog. Surf. Sci.* **71**, 95 (2003).
- <sup>6</sup>F. Rosei, *J. Phys.: Condens. Matter* **16**, S1373 (2004).
- <sup>7</sup>G. Balasundaram and T. J. Webster, *J. Mater. Chem.* **16**, 3737 (2006).
- <sup>8</sup>P. Tambasco de Oliveira, S. F. Zalzal, M. M. Beloti, A. L. Rosa, and A. Nanci, *J. Biomed. Mater. Res.* **80A**, 554 (2007).
- <sup>9</sup>K. Y. Cai, J. Bossert, and K. D. Jandt, *Colloids Surf., B* **49**, 136 (2006).
- <sup>10</sup>F. Schreiber, *Prog. Surf. Sci.* **65**, 151 (2000).
- <sup>11</sup>F. Schreiber, *J. Phys.: Condens. Matter* **16**, R881 (2004).
- <sup>12</sup>J. C. Love, L. A. Estroff, J. K. Kriebel, R. G. Nuzzo, and G. M. Whitesides, *Chem. Rev. (Washington, D.C.)* **105**, 1103 (2005).
- <sup>13</sup>A. Y. Fadeev, R. Helmy, and S. Marcinko, *Langmuir* **18**, 7521 (2002).
- <sup>14</sup>W. Gao, L. Dickinson, C. Grozinger, F. G. Morin, and L. Reven, *Langmuir* **12**, 6429 (1996).
- <sup>15</sup>M. Textor, L. Ruiz, R. Hofer, A. Rossi, K. Feldman, G. Hähner, and N. D. Spencer, *Langmuir* **16**, 3257 (2000).
- <sup>16</sup>E. L. Hanson, J. Schwartz, B. Nickel, N. Koch, and M. F. Danisman, *J. Am. Chem. Soc.* **125**, 16074 (2003).
- <sup>17</sup>E. Hoque, J. A. DeRose, G. Kulik, P. Hoffmann, H. J. Mathieu, and B. Bhushan, *J. Phys. Chem. B* **110**, 10855 (2006).
- <sup>18</sup>C. Viornery, H. L. Guenther, B. O. Aronsson, P. Pechy, P. Descouts, and M. Graetzel, *J. Biomed. Mater. Res.* **62**, 149 (2002).
- <sup>19</sup>E. S. Gawalt, M. J. Avaltroni, M. P. Danahy, B. M. Silverman, E. L. Hanson, K. S. Midwood, J. F. Schwarzbauer, and L. Schwartz, *Langmuir* **19**, 200 (2003).
- <sup>20</sup>M. Nilsing, S. Lunell, P. Persson, and L. Ojamae, *Surf. Sci.* **582**, 49 (2005).
- <sup>21</sup>R. Hofer, M. Textor, and N. D. Spencer, *Langmuir* **17**, 4014 (2001).
- <sup>22</sup>S. Tosatti, R. Michel, M. Textor, and N. D. Spencer, *Langmuir* **18**, 3537 (2002).
- <sup>23</sup>M. Zwahlen, S. Tosatti, M. Textor, and G. Hähner, *Langmuir* **18**, 3957 (2002).
- <sup>24</sup>A. Kanta, R. Sedev, and J. Ralston, *Colloids Surf., A* **291**, 51 (2006).
- <sup>25</sup>R. Quinones, A. Raman, and E. S. Gawalt, *Surf. Interface Anal.* **39**, 593 (2007).
- <sup>26</sup>S. Jalota, S. B. Bhaduri, and A. C. Tas, *Mater. Sci. Eng., C* **27**, 432 (2007).
- <sup>27</sup>J.-H. Yi, C. Bernard, F. Variola, S. F. Zalzal, J. D. Wuest, F. Rosei, and A. Nanci, *Surf. Sci.* **600**, 4613 (2006).
- <sup>28</sup>A. Nanci, J. D. Wuest, L. Péru, P. Brunet, V. Sharma, S. Zalzal, and M. D. McKee, *J. Biomed. Mater. Res.* **40**, 324 (1998).
- <sup>29</sup>D. Brovelli, G. Hähner, L. Ruiz, R. Hofer, G. Kraus, A. Waldner, J. Schlösser, P. Oroszlan, M. Ehrat, and N. D. Spencer, *Langmuir* **15**, 4324 (1999).

- (1999).
- <sup>30</sup>E. S. Gawalt, M. J. Avaltroni, N. Koch, and J. Schwartz, *Langmuir* **17**, 5736 (2001).
- <sup>31</sup>G. A. Niklasson, C. G. Granqvist, and O. Hunderi, *Appl. Opt.* **20**, 26 (1981).
- <sup>32</sup>T. A. Mykhaylyk, N. L. Dmitruk, S. D. Evans, I. W. Hamley, and J. R. Henderson, *Surf. Interface Anal.* **39**, 575 (2007).
- <sup>33</sup>Optical Characterization Group, Universitat de Barcelona, <http://www.ub.es/optmat/>
- <sup>34</sup>N. L. H. Degatica, G. L. Jones, and J. A. Gardella, *Appl. Surf. Sci.* **68**, 107 (1993).
- <sup>35</sup>A. Feng, B. J. McCoy, Z. A. Munir, and D. Cagliostro, *Mater. Sci. Eng., A* **242**, 50 (1998).
- <sup>36</sup>J. R. Hahn and W. Ho, *Phys. Rev. Lett.* **87**, 196102 (2001).
- <sup>37</sup>A. M. Jackson, Y. Hu, P. J. Silva, and F. Stellacci, *J. Am. Chem. Soc.* **28**, 11135 (2006).
- <sup>38</sup>P. K. Ghorai and S. C. Glotzer, *J. Phys. Chem. C* **111**, 15857 (2007).
- <sup>39</sup>J. Pan, H. Liao, C. Leygraf, D. Thierry, and J. Li, *J. Biomed. Mater. Res.* **40**, 244 (1998).
- <sup>40</sup>X. J. Feng and L. Jiang, *Adv. Mater. (Weinheim, Ger.)* **18**, 3063 (2006).
- <sup>41</sup>X. M. Li, D. Reinhoudt, and M. Crego-Calama, *Chem. Soc. Rev.* **36**, 1350 (2007).
- <sup>42</sup>V. R. Kodati, R. El-Jastimi, and M. Lafleur, *J. Phys. Chem.* **98**, 12191 (1994).
- <sup>43</sup>D. M. Spori, N. V. Venkataraman, S. G. P. Tosatti, F. Durmaz, N. D. Spencer, and S. Zurcher, *Langmuir* **23**, 8053 (2007).
- <sup>44</sup>A. H. M. Sondag and M. C. Raas, *J. Chem. Phys.* **91**, 4926 (1989).
- <sup>45</sup>R. Helmy and A. Y. Fadeev, *Langmuir* **18**, 8924 (2002).
- <sup>46</sup>A. Centrone, Y. Hu, A. M. Jackson, G. Zerbi, and F. Stellacci, *Small* **3**, 814 (2007).
- <sup>47</sup>M. D. Porter, T. B. Bright, D. L. Allara, and C. E. D. Chidsey, *J. Am. Chem. Soc.* **109**, 3559 (1987).
- <sup>48</sup>J. B. Schlenoff, M. Li, and H. Ly, *J. Am. Chem. Soc.* **117**, 12528 (1995).
- <sup>49</sup>G. H. Yang, N. A. Amro, Z. B. Starkewolfe, and G. Y. Liu, *Langmuir* **20**, 3995 (2004).
- <sup>50</sup>U. K. Sur and V. Lakshminarayanan, *J. Electroanal. Chem.* **565**, 343 (2004).
- <sup>51</sup>C. L. McGuinness, D. Blasini, J. P. Masejewski, S. Uppili, O. M. Cabarcos, D. Smilgies, and D. L. Allara, *ACS Nano* **1**, 30 (2007).
- <sup>52</sup>L. Richert, F. Vetrone, J.-H. Yi, S. F. Zalzal, J. D. Wuest, F. Rosei, and A. Nanci, "Surface nanopatterning to control cell growth," *Adv. Mater. (Weinheim, Ger.)* (in press).